New European Wind Atlas: The Østerild balconies experiment

Karagali, Ioanna; Mann, Jakob; Dellwik, Ebba; Vasiljevic, Nikola

Published in:
Journal of Physics: Conference Series

Link to article, DOI:
10.1088/1742-6596/1037/5/052029

Publication date:
2018

Document Version
Publisher's PDF, also known as Version of record

New European Wind Atlas: The Østerild balconies experiment

IOP Conf. Series: Journal of Physics: Conf. Series **1037** (2018) 052029 doi:10.1088/1742-6596/1037/5/052029

New European Wind Atlas: The Østerild balconies experiment

Ioanna Karagali, Jakob Mann, Ebba Dellwik, Nikola Vasiljević
Frederiksborgvej 399, Building 125, Risø Campus, DK-4000, Roskilde, Denmark
E-mail: ioka@dtu.dk, jmsq@dtu.dk, ebde@dtu.dk, niva@dtu.dk

Abstract. One of the main objectives of the New European Wind Atlas (NEWA) project is to carry out large scale field experiments at a high spatial and temporal resolution, and provide a significant upgrade to the experimental databases currently available. The Østerild balconies experiment aimed at collecting measurements over a relatively flat and semi-forested terrain to quantify the effect of various terrain features on the mean wind field. The experiment was performed at the Østerild test station for large wind turbines in Northern Denmark, from April to August 2016. The two 250 m meteorological towers available at the test site were equipped with balconies, first at 50 m above local ground level, later raised to 200 m. Scanning lidars were placed on each of the balconies, performing horizontal scans over 90° arcs with an east or west orientation depending on the incoming wind direction. The purpose of this study is to describe i) the new filtering method applied to the data, ii) the wind field reconstruction and the iii) utilisation of the derived wind fields to examine the imprint of surface heterogeneity on the mean wind flow. Cloud point data from aerial lidar scans were used to accurately derive the terrain and tree height. The mean wind flow patterns appeared to be heavily influenced by the terrain characteristics at the height of 50 m above ground level.

1. Introduction

The aim of the New European Wind Atlas (NEWA) project is the creation and publication of a European wind atlas of unprecedented accuracy [1, 2]. The project is structured around two areas of work: development of down-scaling methodologies combining models of large-scale atmospheric flow to local flow at any potential wind turbine site [3], and measurement campaigns to validate such methodologies. A description of the entire project is available in [4]. Characteristic sites in various landscape types over Europe were selected for the measurement campaigns covering offshore, coastal, forested and hilly/mountainous terrains [5]. The experiment described in this study is motivated by often seen uncertainties in the estimated wind energy potential over terrain covered by forest [6]. In the vicinity of forest edges the flow may be even more difficult to predict which has led to detailed experimental campaigns of the flow around such an edge [7]. The combination of hills and patchy forest may be particularly difficult to predict [8] but here we concentrate on patchy forest on a flat underlying surface.

Scanning Doppler lidars have been used before to investigate atmospheric flow for wind energy purposes. A single lidar was scanning horizontally forth and back over a forest edge showing a speed up right over the edge [7]. Later a single scanning lidar made rapid wind profiles close to the ground over the Bolund peninsula [9] showing a sharp, rapidly varying limit between the very turbulent flow generated by the escarpment and the oncoming flow. More recently multiple

synchronised lidars were used to measure the turbulent flow over a forested hill in Germany for comparisons with more traditional mast based sonic measurements [10]. During the pilot Perdigo Experiment, [11], synchronised lidars were used to compare the flow over the parallel ridges with linked micro- and meso-scale flow models [12], understand the inflow towards a wind turbine situated in this complex terrain [13], and show the wind turbine wake dependence on atmospheric stability and impact on the re-circulation behind the ridge [14].

During the Østerild balconies experiment, two horizontally scanning Doppler lidars were used to obtain overlapping, horizontal scans at 50 and 200 m above the ground over a period of five months, during spring and summer of 2016, with the aim of characterising the impact of heterogeneous forest on the mean flow at turbine relevant heights. During post-processing of the data, an adapted filtering approach was introduced based on [15] to increase the amount of availability. Instantaneous scans were filtered and the horizontal wind field was calculated. The mean wind flow for various wind direction sectors was computed in order to assess the impact of the terrain characteristics. In this study, the focus is on measurements obtained during the first phase of the experiment, i.e. at 50 m above ground level, as the impact of the terrain is expected to be higher closer to the ground. In this manuscript the data, experimental set-up, along with the filtering and reconstructing methodologies are presented in Section 2. The results are presented and discussed in Section 3 while the findings are summarised in Section 4.

2. Data and Methods

2.1. Lidar instruments

The long-range WindScanner system [16] is primarily designed for measurements of atmospheric mean flow fields. It is a configuration of two or more spatially separated pulsed scanning lidars controlled by a remote master computer. The WindScanners have been specifically tailored to perform user-defined and time-controlled scanning trajectories in a synchronised mode. Since WindScanners are based on the pulsed technology they have a large full-width half-maximum probe length (minimum 25 m) and low measurement frequency (typically 1 Hz). They are capable of retrieving the radial wind speed measurements up to 8 km in range [17]. WindScanners can simultaneously retrieve radial velocity from up to 500 range gates distributed along the laser light propagation path.

2.2. Meteorological mast data

The two light towers, located at the Østerild test station for large wind turbines, are installed in a south-north orientation at a distance of 4.25 km. They are 250 m high and equipped with various instruments. For the purpose of the present study, 10 minute mean measurements of wind speed and direction from sonic anemometers (uSonic-3Basic, Metek Gmbh, Hamburg) at 37 m were used to categorise the incoming wind flow conditions. The time-series of measurements from the light towers are shown in Figure 1, where it is seen that the north tower (orange) suffers from a lack of data during the first part of the experimental campaign. Thus, only the south tower time-series was used to separate the reconstructed wind fields from the WindScanners to 12 distinct wind direction bins using a step of 30°, the first of which was centred at 0° and the last at 330°.

2.3. Experimental set-up

2.3.1. Instrument installation The measurement campaign lasted from April to August 2016. One balcony-type platform was installed on each of the light towers, at 50 m above ground level (agl) during Phase 1, and 200 m during Phase 2 (see Table 1). Scanning lidars were placed at each of the platforms and levelled according to their dual-axis inclinometers. The static pointing accuracy of the instruments was assessed by mapping the Carrier-to-Noise Ratio (CNR) of targeted landmarks. Due to previous calibration, the north instrument showed a

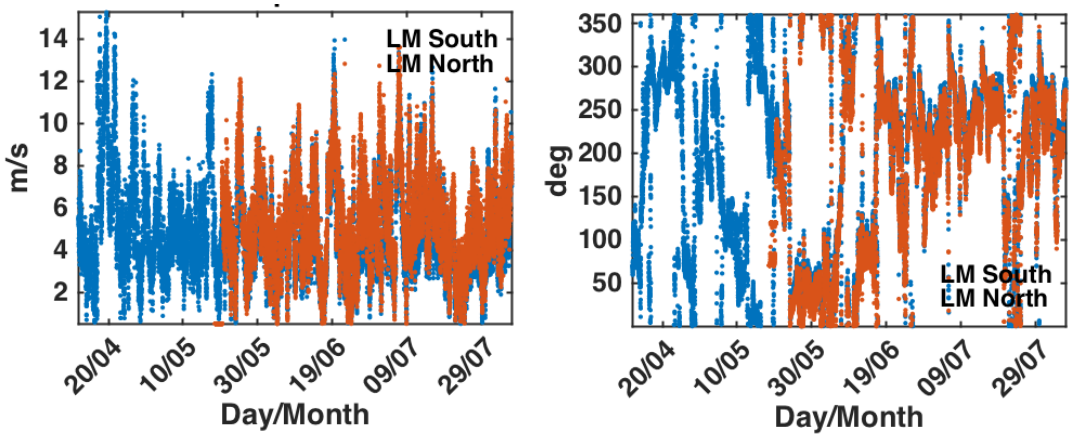

Figure 1. Time-series of wind speed (left) and direction (right) for the 37 m level.

proper fit of the mapped and referenced targets. This was not the case for the south instrument, resulting in the laser beam to hit the ground at zero elevation although the instrument was installed at 50 m above the ground.

Assuming that the static pointing error originated only from the imperfect levelling and home position offset, one would expect the elevation error to follow a sine curve for the full range of azimuth angles. Thus, the azimuth positions of five well distributed targets, i.e. a chimney at 50°, a wind turbine at 120°, two Range Height Indicator (RHI) scans at 255° and 286° and the north light mast at 355° were used to estimate elevation errors, allowing the derivation of the sine curve (Figure 2). This was encoded in the motion controller of the instrument, to compensate for the imperfect levelling, thus improving the pointing accuracy.

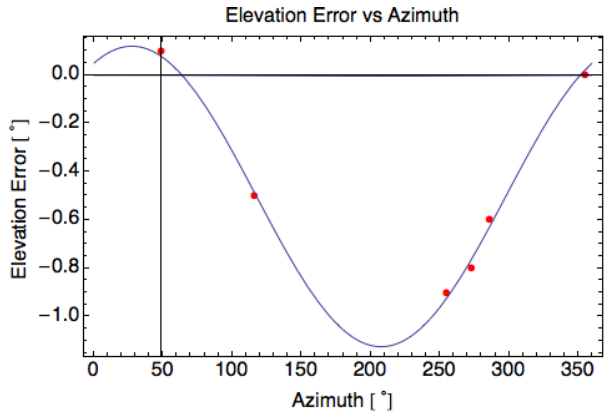

Figure 2. The sinusoidal fit of the elevation error.

2.3.2. Scanning patterns Two mirror-imaged scanning patterns were implemented, during which the scanners were synchronously scanning the same horizontal plane which allowed to perform reconstruction of the horizontal wind vector. A total of 45 Line-Of-Sight (LOS) directions covering in total 90° with 198 range gates for each LOS were used. The closest range gate was at 105 m from the instruments and the furthest at 7000 m, using a range gate step of 35 m. The full-width half-maximum of the measurement volume was approximately 75 m and the accumulation time was one second, thus one full scan of the horizontal plain was obtained in 45 seconds.

Table 1. Time-line of the experiment. The date and time format follows the convention YYYY-MM-DD HH:MM:SS.

Phase #	Measurement Start	Measurement End	Length
1: 50m AGL	2016-04-12 12:45:41	2016-06-17 12:48:01	66 days (1584 hours)
2: 200m AGL	2016-06-29 13:35:56	2016-08-12 09:09:55	43.8 days (1051 hours)

During the east scanning pattern, the north scanner started at 75° (geographical) and gradually scanned clockwise to 165° with a speed of 2°/s. The south scanner started synchronously at 105° and gradually scanned anti-clockwise to 15° at a speed of -2°/s. After a full scan, both scanner heads returned to their initial positions and synchronous scanning was resumed. For the west scanning pattern the arrangement was mirrored, i.e. the north scanner started at 285° and gradually scanned anti-clockwise to 195° while the south scanner started from 255° and scanned clockwise to 345°, both with a speed of 2°/s, see Table 2 and Figure 3.

Table 2. Locations, in UTM 32-ETRS89, of the north and south towers along with the range of azimuth values for each scan type, i.e. west and east. The number in brackets reflects the step between azimuth angles.

Scanner	Location		Scanning pattern	
	Eastings	Northings	west	east
south	492768.8	6322832.3	344°-256° (-2°)	16°-104° (2°)
north	492768.7	6327082.4	196°-284° (2°)	164°-76° (-2°)

The east and west scanning patterns alternated depending on the incoming wind conditions, which were physically inspected by a WindScanner operator. Once the incoming wind direction changed, then the instruments were also programmed to change scanning patterns. This change of scanning patterns, amongst other reasons, resulted in restarting the instruments thus measurements were obtained in sessions, defined as continuous periods of uninterrupted recording.

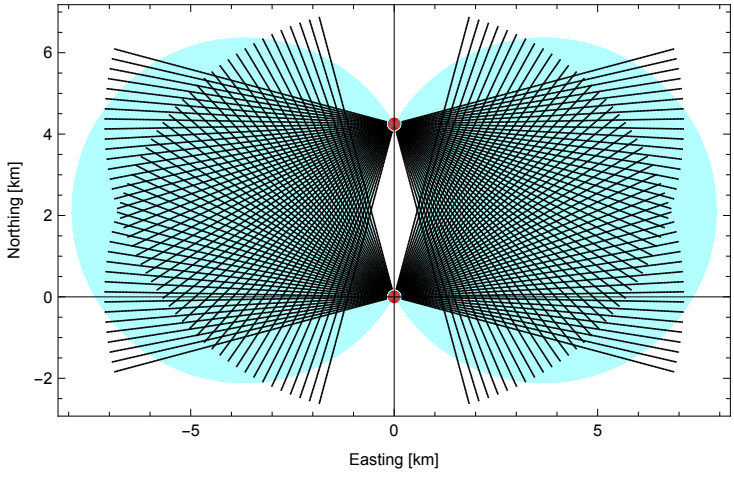

Figure 3. Graphical representation of the two scanning patterns. Positions are relative to the south mast. In the blue area the angle between the beams is more than 30°.

2.4. Aerial lidar scan

The freely available point cloud data from a national survey of terrain height from Geodatastyrelsen, Denmark, (`http://download.kortforsyningen.dk/`) were used to make an accurate description of the site and its land cover. The aerial scans for the Østerild area were obtained during November-December 2015. The point cloud data were used to estimate the tower positions (Table 2) and create maps of the terrain height, vegetation height and water areas relative to the position of the southernmost tower for a 20 km $\times$ 10 km area surrounding the towers with a resolution of 10 m resolution, using the approach presented in [18].

2.5. WindScanner data filtering

Radial speeds were filtered to remove ambiguous measurements, due to hard targets and other effects. Each 45-second scan was treated individually, thus filtering and reconstruction occurred at a 45 s basis. The filtering method applied was based on [15]. For each Line-Of-Sight (LOS) in a 45 s scan, the median of radial wind speed values from all range gates was used as a filter. If the absolute difference between the radial wind speed of a given range gate and the median value for this LOS, $|LOS - LOS_{median}|$, exceeded a certain threshold, then the LOS speed for the given range gate was discarded.

To identify this dynamic filtering threshold, density scatter-plots of the $|LOS - LOS_{median}|$ versus the CNR values were examined. An example is shown in Figure 2.5, using 7243830 measurement points. It presents a dipole shape, with most points - or highest data density - observed for the interval between the two grey lines, i.e. for $|LOS - LOS_{median}| < 3\ \mathrm{m\,s^{-1}}$, which was selected as a threshold for further filtering.

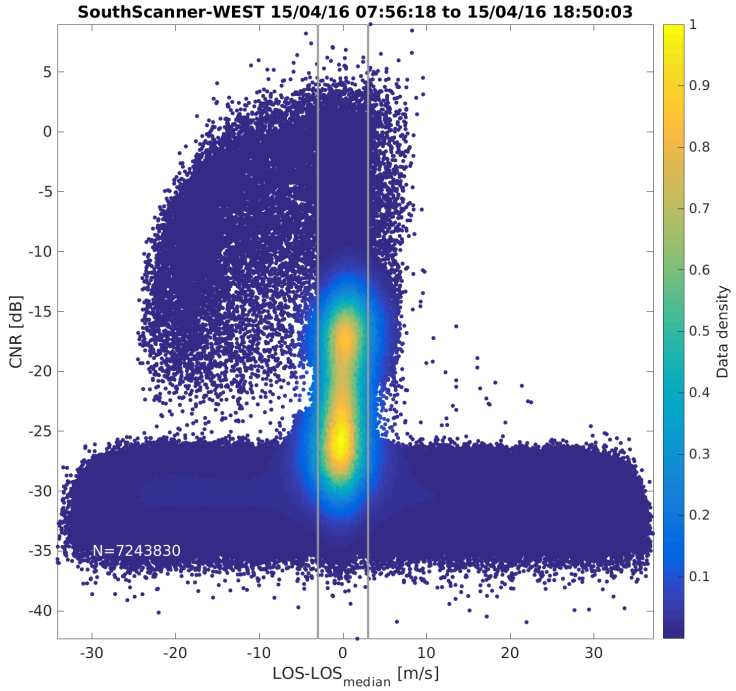

Figure 4. Density scatter plot of the $|LOS - LOS_{median}|$ as function of the carrier-to-noise ratio (CNR), for a measurement session from the south instrument on April 15 2016. The grey vertical lines represent the filtering threshold of 3 $\mathrm{m\,s^{-1}}$.

2.6. Wind field reconstruction

A grid around the south instrument was defined, extending 7000 m to the east and west directions, 1500 m to the south and 5700 m to the north, with a grid spacing of 100 m. The grid was transformed to polar coordinates, such that any given point was associated to the north and south scanner as a function of distance and angle. Each LOS azimuth angle was associated

to a specific angle from the reference matrices. For a specific LOS, the range gate distances were associated to distances from the reference grids. This was performed separately for each instrument. In the case when a grid point from the angle reference array fell between two LOS azimuth angles, the mean azimuth angle was used and consequently the mean LOS wind speed. In the case when a grid point from the distance reference array fell between two range gates, the mean value of the two LOS speeds associated with these range gates was used.

Finally the reference arrays were populated with the corresponding LOS wind speeds for each instrument, i.e. two LOS speed values for any given grid point at best. For a reconstruction to occur at a specific point, *(i,j)*, of the reference grid, a set of LOS wind speeds were required, one from each instrument. For the points where this condition was valid, the horizontal (u) and vertical (v) wind components were estimated following the Equations 1 and 2, where θ_1 and θ_2 are the azimuth angles of the south and north scanner and u_{LOS1}, u_{LOS2} are the LOS wind speeds from the two scanners, respectively.

$$u_{i,j} = \frac{-u_{LOS1} \times \sin(\theta_2) + u_{LOS2} \times \sin(\theta_1)}{\sin(\theta_1 - \theta_2)} \tag{1}$$

$$v_{i,j} = \frac{u_{LOS1} \times \cos(\theta_2) - u_{LOS2} \times \cos(\theta_1)}{\sin(\theta_1 - \theta_2)} \tag{2}$$

The wind speed $U_{i,j}$ and direction $Dir_{i,j}$ at a specific point i,j were estimated using Equations 3 and 4:

$$U_{i,j} = \sqrt{u_{i,j}^2 + v_{i,j}^2} \tag{3}$$

$$Dir_{i,j} = 270 - \arctan(v_{i,j}, u_{i,j}) \tag{4}$$

3. Results

3.1. Filtering and data availability

Figure 5, left, shows an example of a density scatter-plot using all available measurements from a 12-hour session of the south scanner. The scatter-plot shows the density, or availability, for a radial speed of certain value and its corresponding CNR value. Thus, it provides information about the most frequently recorded radial speed values (x-axis) and their given Carrier-to-Noise Ratio (CNR) values (y-axis). It presents a dipole shape, with most radial speeds - or highest data density - observed between the interval -10 $\mathrm{m\,s^{-1}}$ to 8 $\mathrm{m\,s^{-1}}$, and for a CNR range of -12 dB to -33 dB. Note that negative radial speed values signify that the direction of the incoming flow is towards the lidar beam. The grey lines represent two fixed filtering thresholds, i.e. -27 dB (solid) and -28 dB (dashed), to depict the approach of a fixed CNR range for filtering WindScanner data. If such thresholds were applied, all radial wind speeds with CNR values outside the predefined range would be discarded, including a large amount of measurements at the lower part of the dipole of highest data density. From a total of 7243830 measurements 75.5% of data would be maintained using the =27 dB threshold, and 83% when using the =28 dB threshold.

Figure 5 (right) shows the density scatter-plot when the new filtering approach was applied. The dipole structure is maintained while scattered points around it have been completely removed. With this approach the final number of available points was 6684987, thus 92.3% of the original points were maintained. This demonstrates the more selective nature of this filtering approach, where almost the entirety of "noisy" measurements is discarded while maintaining the dipole structure of highest data density.

This is further demonstrated in the example shown in Figure 6. The original radial speed field from a single scan of the south instrument is shown in (a) along with the resulting field after filtering with a fixed CNR range between -8 and -27 [dB], (b), while the one filtered using the dynamic approach is shown in (c). Note the flow field scan is presented in the co-ordinates

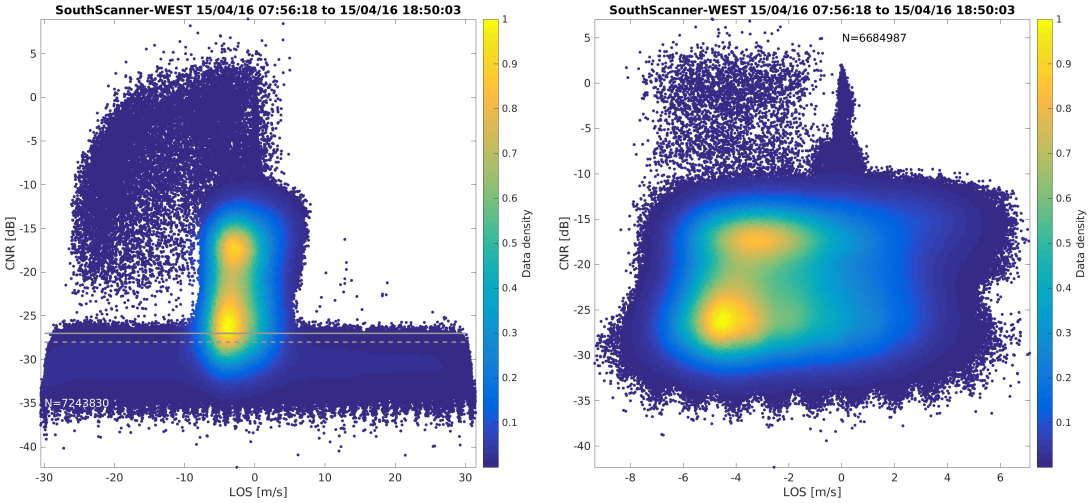

Figure 5. Density scatter plot of the radial speeds as function of the carrier-to-noise ratio, for a measurement session from the south instrument on April 15 2016. The grey lines represent filtering thresholds using a fixed value approach (left). Filtered data when using the $|LOS - LOS_{median}|$ approach (right).

of the WindScanner, i.e. the x-axis represents distance from the instrument while the y-axis indicates the azimuth angle of the lidar beam. While applying the dynamic filtering approach, isolated range gates with missing information could occur due to random causes, e.g. a bird, and thus interpolation was performed to provide missing information for such isolated cases. Gap filling for a specific range gate was performed, only if the surrounding range gates had a valid measurement, by using the estimated mean LOS wind speed value between the previous and next range gate.

The original scan shows a relatively uniform field of LOS values with an area of randomly varying radial speeds, at the far end of the scan field, starting at 5.6 km away from the instrument. Note the diagonal of range gates with very low radial speed values located between 2.5 km and 3.5 km, associated to a row of wind turbines acting as hard targets which reflect the laser beam directly back to the scanner. When the fixed CNR range filtering was applied, in (b), most of the "noisy" measurements at the far end of the scan field were discarded with few exceptions, while the hard targets still remained unfiltered. In addition, extensive filtering seemed to occur as the area of missing data in Figure 6b is extended compared to the area of "noisy" measurements in Figure 6a. To the contrary, when the "dynamic" filtering was applied (Fig 6c), range gates with very high absolute radial speed values were discarded. Such cases mostly occurred at distances beyond 4.9 km. In addition, fewer measurements were discarded using the dynamic filtering approach while the series of very high LOS speeds due to the row of wind turbines, was successfully filtered in Figure 6c, which also demonstrates that the applied interpolation did not actually interfere with successfully filtered measurements.

Phase 1 of the campaign lasted 66 days, corresponding to a maximum of 126720 45 s scans. The south scanner obtained 97624 45 s scans, accounting for 77% data availability while there were 90695 45 s scans obtained from the north scanner, i.e. 71.57% data availability. After applying the filtering criteria and reconstructing the available 45 s scans, the data availability was estimated as the maximum number of reconstructions for any given point during each measurement session, along with the median and mean number of reconstructions for the same session. All points with zero reconstructions were discarded, while the size of the reconstructed area was also estimated. Figure 7 shows for each of the 60 measurement sessions of Phase 1

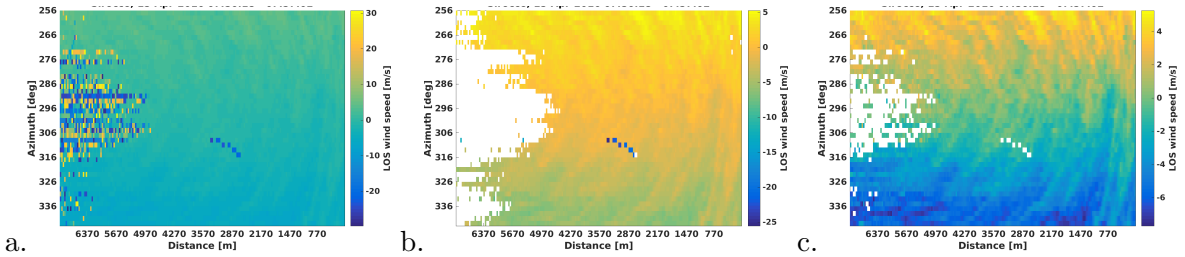

Figure 6. Radial wind speed from the south scanner for one 45-s scan when (a.) no filtering was applied, (b.) the fixed −8 to −27 range was applied and (c.) the dynamic filtering was applied.

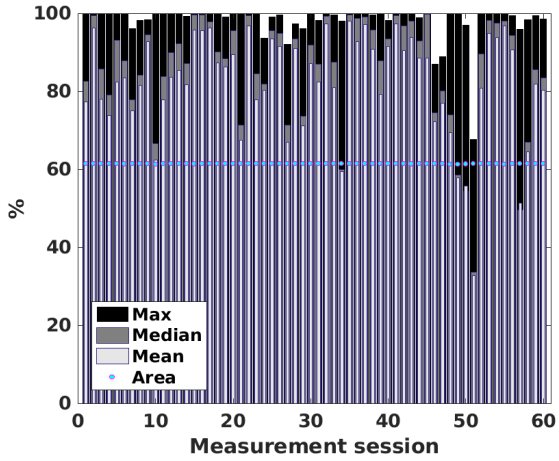

Figure 7. Statistics of data availability for all the measurement sessions during Phase 1.

(x-axis), the maximum percentage of reconstructions (black bars) which may occur for only one or more points in the scanned area. Since this maximum % could occur for only one or very few points, the mean (white) and median (grey) percentages along with the percentage of reconstructed area (dots) are also shown. The maximum percentage of the reconstructed wind field is constant for all measurement sessions at ∼61%. While the maximum percentage of reconstructions for each session is almost always above 90%, the median is around 85% which signifies a rather high data availability of reconstructed winds.

3.2. Terrain features

The cloud point data were used to map terrain characteristics of interest to the present study. The bottom panels of Figure 8 show the derived tree height (left) and terrain height (right). According to the latter, there is a difference of the terrain height between the south and north light towers of 6.6 m. Brighter colours indicate higher ground while darker colours are representative of either water surfaces or flat, non-vegetated terrain. Note the existence of various terrain features, e.g. a forested hill at 5 km east and 3 km north of the south light tower. An escarpment is found 5 km to the west and about 2 km north of the south light tower, while further escarpments can be identified further away and well outside the scanned area. Moreover, the North Sea and a fjord type structure can also be identified as very dark areas at the north and south-east directions.

3.3. Mean flow

Using the wind direction at 37 m from the south light mast, all available reconstructed wind fields were separated in the 12 distinct wind direction bins. The mean wind over the entire period

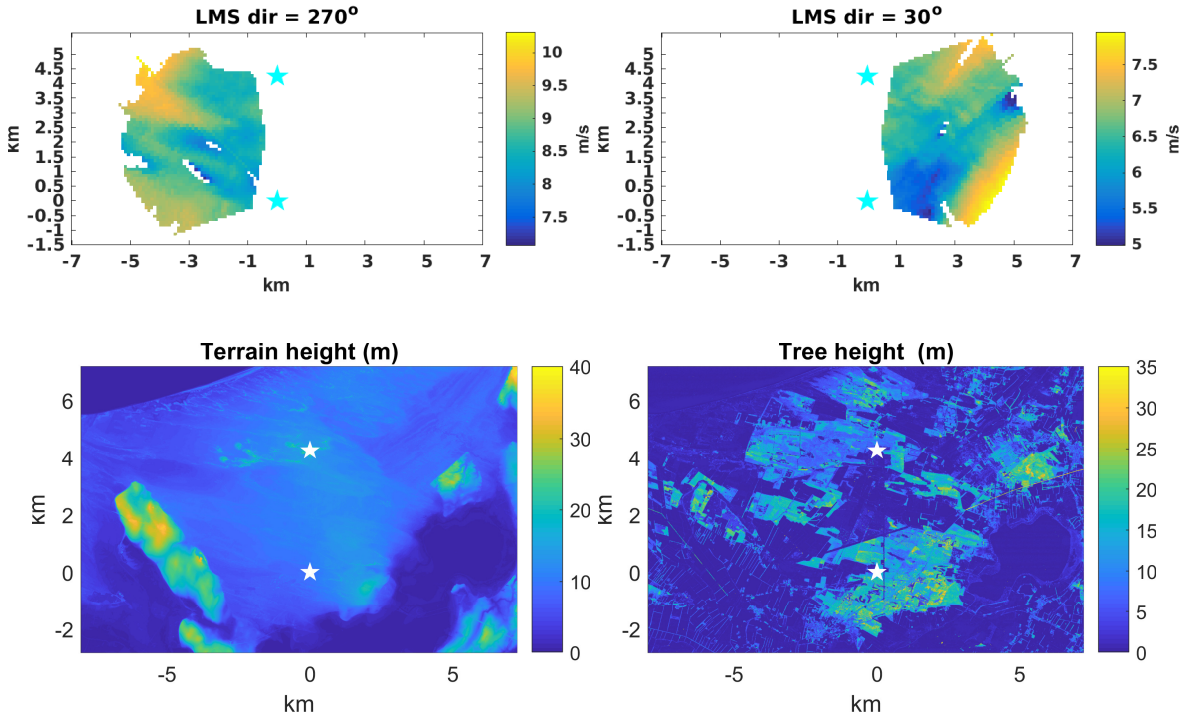

Figure 8. Mean wind speed at 50 m for incoming wind flow from the west (left) and north-east (right) according to the south light mast (LMS) direction, along with the tree and terrain height maps from the cloud point data (bottom).

of available data was estimated for each wind direction bin. As different number of reconstructed wind speeds was used at each range gate and for each wind direction bin, depending on the data availability, this study will focus on the dominant wind directions. For incoming wind from the 30° and 270° bins (±15°), the mean wind speed is shown in the top panels of Figure 8. The minimum and maximum number of measurements used for the averaging were 8015 and 10237 for the 30° bin, while the minimum and maximum number for the 270° bin were 9426 and 10430, correspondingly. Thus the dominant wind directions for the measurement campaign at 50 m were westerly and north-easterly winds, also confirmed by the right panel of Figure 1.

The top left panel of Figure 8 shows the mean wind speed at 50 m above the ground when the incoming wind at the south light tower is from the west, i.e. 270° ±15°. If examined in parallel with the bottom panels showing the terrain and tree height of the area, the impact of the terrain on the mean wind flow is evident. The region of higher mean wind of ∼10 $\mathrm{m\,s^{-1}}$ appearing in the north-west part corresponds remarkably well with the area of very low terrain elevation around 5 km west and 4 km to 6 km north of the south light tower. Moreover, the higher points located ∼5 km west and 2 km to 3 km north of the south light tower cause a reduction in the amplitude of the mean wind flow, which recovers further south when the terrain becomes flatter and the vegetation lower. The top right panel of Figure 8 shows the mean wind for the direction bin of 30° ±15°, corresponding to north-east winds. The "fingerprint" of the lower areas located approximately 5 km east of the south light tower that correspond to the Tømmerby fjord appears as an area with higher wind speeds on the mean flow field. To the contrary a significant reduction and speed-up is identified around the escarpment located 5 km east and ∼2 km north of the south light tower. Characteristic is also the reduced mean flow

directly east of the south light tower, where the terrain is forested.

4. Conclusions

This study provided the description of an experimental campaign utilising two WindScanner instruments to simultaneously record radial wind speeds over a relatively flat nonetheless semi-forested, and with the existence of escarpments, terrain at two different heights above the ground, at 50 m and 200 m. When available, the simultaneous scans were used to reconstruct the wind field over the area in order to examine the potential signature of the terrain features on the mean wind flow. Extensive filtering sensitivity tests were performed prior to the reconstruction of the wind fields, aiming at identifying the optimal method to remove ambiguous measurements while maintaining the highest possible data availability. It was found that following a "dynamic" approach to filter the data, that depended on the actual characteristics of the measurement campaign, i.e. the recorded radial speeds, rather than adopting a fixed ratio of values to filter out for, resulted in maintaining a higher data density while removing ambiguous values. Nonetheless, the selected filtering threshold depended on the wind flow characteristics and thus its sensitivity could be further investigated. The data obtained at 50 m above the ground were used to perform wind field reconstruction of the 45 s scans and were categorised according to the incoming wind as measured from a sonic anemometer located 37 m above the ground, on the south light tower. The directions with the highest data availability were west and north-east, for which the mean wind flow showed a clear influence by the terrain characteristics. The impact of flat, non-vegetated areas, escarpments, water bodies and forested terrain was distinct with higher mean wind speeds over flat and bare terrain and lower mean wind speeds over forested areas.

Acknowledgments

Our colleagues N. Angelou, G. Lea, E. Simon and all technical staff are thanked for their efforts to install and monitor the instruments and distribute the data.

References

[1] Petersen E L, Troen I, Jørgensen H E and Mann J 2013 *Environ Res Lett* **8** 011005
[2] Petersen E L 2017 *J Renew Sustain Ener* **9** 052301
[3] Sanz Rodrigo J, Chavez Arroyo R A, Moriarty P, Churchfield M, Kosović B, Réthoré P E, Hansen K S, Hahmann A, Mirocha J D and Rife D 2017 *WIRES Energy Environ* **6**
[4] Calamia J 2017 *New Sci* **234** 31–33
[5] Mann J, Angelou N, Arnqvist J, Callies D, Cantero E, Arroyo R C, Courtney M, Cuxart J, Dellwik E, Gottschall J *et al.* 2017 *Phil Trans R Soc A* **375** 20160101
[6] Dellwik E, Landberg L and Jensen N O 2006 *Wind Energy* **9** 211–218
[7] Dellwik E, Bingöl F and Mann J 2013 *Q J Meteor Soc* **10.1002/qj.2155**
[8] Montavon C 1998 Ph.D. thesis École Polytechnique Fédérale de Lausanne
[9] Lange J, Mann J, Angelou N, Berg J, Sjöholm M and Mikkelsen T 2015 *Bound-Lay Meteorol* 1–13
[10] Pauscher L, Vasiljevic N, Callies D, Lea G, Mann J, Klaas T, Hieronimus J, Gottschall J, Schwesig A, Kühn M *et al.* 2016 *Remote Sens-Basel* **8** 782
[11] Vasiljević N, Palma J M, Angelou N, Matos J C, Menke R, Lea G, Mann J, Courtney M, Ribeiro L F and Gomes V M 2017 *Atmos Meas Tech* **10** 3463
[12] Rodrigues C V, Palma J, Vasiljević N, Courtney M and Mann J 2016 *J Phys Conf Ser* vol 753 (IOP Publishing) p 032025
[13] Forsting A M, Bechmann A and Troldborg N 2016 *J Phys Conf Ser* vol 753 (IOP Publishing) p 032041
[14] Menke R, Vasiljević N, Hansen K S, Hahmann A and Mann J 2018 *Wind Energy Science* Submitted
[15] Beck H and Kühn M 2017 *Remote Sens-Basel* **9** 561
[16] Vasiljević N, Lea G, Courtney M, Cariou J P, Mann J and Mikkelsen T 2016 *Remote Sens-Basel* **8**
[17] Floors R, Peña A, Lea G, Vasiljević N, Simon E and Courtney M 2016 *Remote Sens-Basel* **8**
[18] Floors R, Enevoldsen P, Davis N, Arnqvist J and Dellwik E 2018 *Wind Energy Science Discussions* 1–29 URL `https://www.wind-energ-sci-discuss.net/wes-2018-10/`